Probability of Unrecognized LiDAR Interference for TCSPC LiDAR

Sara Grollius, Andre Buchner, Manuel Ligges, and Anton Grabmaier

***Abstract*—A standard method for distance determination is light detection and ranging (LiDAR), which relies on the emission and detection of reflected laser pulses. When LiDAR systems become common for every vehicle, many simultaneous laser signals will produce mutual LiDAR interference between LiDAR systems. In this paper, we analyze the possibility to recognize mutual interference in time-correlated single photon counting (TCSPC) LiDAR with particular focus on flash systems. We evaluate the LiDAR interference appearance by deriving the expected event distribution for ego and aggressor signal. From that, we calculate the probability of photon detection within each measured signal. This paper shows the high potential of different pulse repetition frequencies to reduce LiDAR interference. Using signal-to-noise ratio (SNR), we define the extinction distance, beyond which the aggressor signal completely extinguishes the ego signal. Applied on different background and laser event rates, we find the connection between ideal LiDAR system designs and lowest probability for unrecognized LiDAR interference. Furthermore, we show the relationship to a specific LiDAR design, which must fulfill eye safety condition and receives lower intensities with increasing target distances. Finally, we present different solutions for the recognition and reduction of LiDAR interference based on our previous results.**

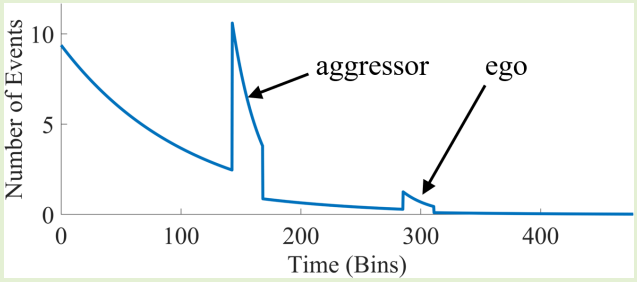

***Index Terms*— Light detection and ranging (LiDAR), mutual LiDAR interference, time-correlated single-photon counting (TCSPC), direct time-of-flight (dTOF).**

I. Introduction

LIGHT detection and ranging (LiDAR) is a promising technique for applications requiring distance measurements like autonomous driving. LiDAR systems emit laser light that is reflected by targets in the vehicle's environment. Multiple LiDAR systems at the same location can cause mutual LiDAR interference. With the term "LiDAR interference", we refer only to mutual distortions between the LiDAR systems itself and not the measurement of background photons like sunlight. In this work, we focus on the interference between TCSPC flash LiDAR systems in the presence of background light. For scanning systems, the asynchronous beam steering complicates the simultaneous target observation and hence strongly reduces the probability of LiDAR interference [1], [2]. This scanning movement is not discussed in this work. The measurement principle TCSPC can be used for the LiDAR method direct time-of-flight (dTOF), where short laser pulses travel to the target and afterwards back to the LiDAR system. For dTOF, the target distance d can be directly determined by the time-of-flight (TOF) t_{TOF} of a reflected laser pulse and the known speed of light c to

$$d = \frac{c \cdot t_{\mathrm{TOF}}}{2}. \tag{1}$$

LiDAR systems can measure the arrival times of single photons, which is called TCSPC. For this purpose, a time-to-digital converter (TDC) can be used, which counts the time in defined timing resolution, e.g. 312.5ps corresponding to a distance resolution of 5cm.

Besides real photons, there is a dark count rate (DCR) indicating the number of events per second induced intrinsically in the sensor. Furthermore, the presence of background light produces events in the sensor. Often, the DCR is negligible compared to the background event rate. Hence, we ignore it in the following considerations. However, if the DCR should be considered as well, events caused by the DCR or background light can be summarized as common noise event rate. In the following, we define the laser and background event rate as events per second in the sensor caused by laser photons and background

Manuscript received April 13, 2022; revised May 16, 2022; accepted May 23, 2022. Date of publication June 8, 2022; date of current version July 1, 2022. The associate editor coordinating the review of this article and approving it for publication was Dr. Anuj K. Sharma. *(Corresponding author: Sara Grollius.)*

Sara Grollius, Andre Buchner, and Manuel Ligges are with the Fraunhofer Institute for Microelectronic Circuits and Systems, 47057 Duisburg, Germany (e-mail: sara.grollius@ims.fraunhofer.de).

Anton Grabmaier is with the Department of Electronic Components and Circuits, University of Duisburg-Essen, 47057 Duisburg, Germany, and also with the Fraunhofer Institute for Microelectronic Circuits and Systems, 47057 Duisburg, Germany.

Digital Object Identifier 10.1109/JSEN.2022.3178179

photons respectively. The LiDAR system cannot distinguish if a single event is generated by a laser or a background photon. To distinguish them, single photon measurements are accumulated and histogrammed for further analysis.

After each event, the sensor becomes insensitive for a specific time. This dead time can be longer than the laser pulse width. In this case, after one laser photon detection, no further laser photon can be detected. Here, we assume that only the first photon of each measurement is acquired. Therefore, the maximum number of accumulated measurements is equal to the number of emitted laser pulses. All measured photon arrival times are combined in one histogram. Two example histograms are shown in Fig. 1, which is explained in section III in more detail. The underlying event rate contains a moderate background event rate of $r_B = 30$MHz demonstrating the typical background distribution in Fig. 1 [3]–[5]. Additionally, laser signals with laser event rate $r_L = 100$MHz increase the total event rate temporarily. These rates are transformed in histograms with exponential event distribution, which is often called "pile-up" and is explained later in section III [6]–[8]. The histogram has a bin width corresponding to the timing resolution of the TDC. In this figure, the bin width of 312.5ps is so small that the distribution of the expected events appears smooth. From this histogram, the TOF of the total laser signal is determined by a suitable algorithm.

The following investigations are performed considering a few assumptions. For LiDAR interference, identical systems are more critical than different ones. Equivalent to this, identical targets observed by these LiDAR systems are assumed. For example, most LiDAR systems use spectral filtering by bandpasses with narrow spectral width, so that all wavelengths outside this bandpass filter width are filtered out. Hence, only systems operating at the same wavelength produce mutual interference. Furthermore, operation at different pulse repetition frequencies attenuates interference because a single foreign photon will hardly be recognized in a total histogram but continuously interfering measurements will accumulate. The same effect is expected for multiples of the pulse repetition frequency but in a weaker form.

Considering a world full of vehicles with LiDAR systems, the mutual interference between LiDAR systems can be crucial. In the future, maybe only a few LiDAR systems will establish themselves on the LiDAR market so that it becomes very probable that two vehicles with the same LiDAR system will meet. There is an increasing research on LiDAR interference with regards to different LiDAR methods. For short-pulsed LiDAR using common photodetectors like avalanche photodiodes (APDs), code-division multiple access (CDMA) is used in the form of modulating the pulse form [9] or using pulse trains instead of single pulses [10], [11]. TCSPC LiDAR using single-photon detectors like single-photon avalanche diodes (SPADs) underlie dead times and are thus often restricted to first-photon measurements. TCSPC systems focus on LiDAR interference approaches like pulse-position modulation (PPM) [12]–[17] or CDMA realized by dual-pulse emission considering dead time [18]. One paper even combines CDMA and PPM applied to scanning LiDAR [19]. To our knowledge, we are the first to investigate

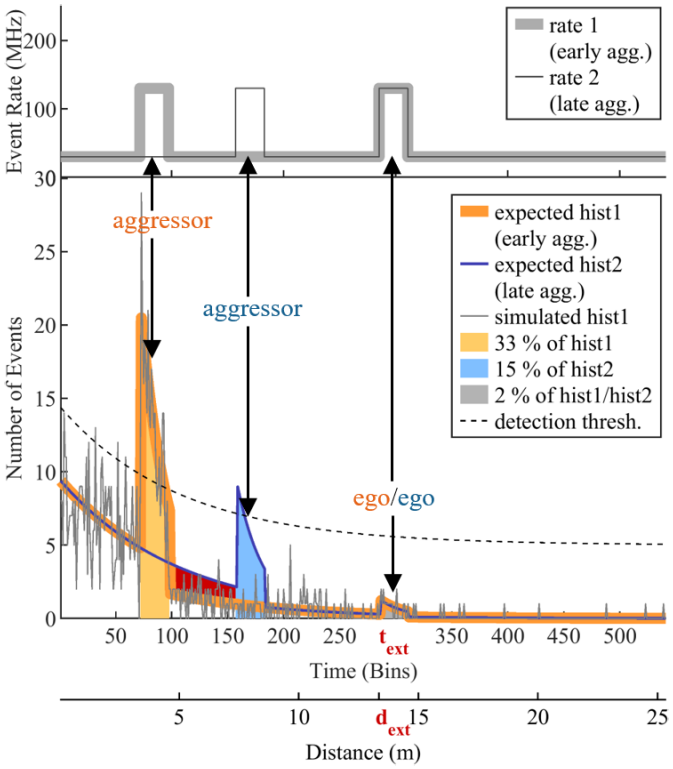

Fig. 1. Two example histograms with different TOFs of the aggressor signal resulting into the same extinction TOF t_{ext} or extinction distance d_{ext} of the ego signal, which is below the detection threshold. In both cases, background and laser event rate are $r_B = 30$MHz and $r_L = 100$MHz. The integrals of both expected histograms are the same so that the orange aggressor is higher over background than the blue one but the blue background is increased by the red area instead. The ego signal has the same position and height for both histograms because it is independent of the aggressor position and height. The ego signal is not recognizable anymore within the noise, which is shown by simulation of the orange histogram.

interference considering strong background light, which can lead to unrecognized LiDAR interference. In the following, the LiDAR interference of identical LiDAR systems is analyzed, both with TCSPC measurement and first-photon acquisition. We focus on flash LiDAR systems, which means no investigation of scanning patterns and hence a higher probability of LiDAR interference. Throughout this work, the investigated LiDAR system is called ego LiDAR system, whereas other LiDAR systems are declared as aggressor LiDAR systems.

For the following analysis, the default parameters used for calculations and figures are shortly described. The most important parameters are additionally listed in the appendix. As most targets reflect light in a diffuse manner, reflections following the Lambertian law are assumed in the calculations. The highest target reflectance of $\rho = 100\%$ is chosen as an edge case. Assuming a target distance of $d = 10$m, the previous parameters can be equated to a laser event rate of about $r_L = 100$MHz received at the sensor [20]. A typical number of accumulated measurements $n_{meas} = 1000$ is applied. A distance determination method is assumed that requires a minimum SNR $k_{SN,min} = 3$ for a successful target detection [21]. The SNR is discussed later in more detail. A moderate background of $r_B = 30$MHz is chosen. In general, LiDAR interference can also occur in the absence

of background illumination, which is described by the derived equations in this work as well. Although mathematically possible, the background should not be chosen to an ideal value of 0Hz, as this unrealistic value would lead to unrealistically high measurement distances. In reality, there is always a minimal noise floor, which is technically given by the DCR electrically producing false detections. As not declared otherwise, these parameters are used as default in the following calculations and diagrams.

This paper is structured as follows. In section II, the direct and indirect LiDAR interference are defined and compared. In section III, we obtain the appearance of interference in the histogram, which is analyzed with respect to distance determination and possible asynchronicity between LiDAR systems. In section IV, we determine unrecognized LiDAR interference for different scenarios, where subsection IV-A derives required equations, IV-B varies background and laser intensities and IV-C assumes a specific LiDAR system underlying eye safety restrictions. Section V processes the investigations to possible solutions for recognition and reduction of LiDAR interference.

II. LiDAR Interference Types

For identical LiDAR systems, LiDAR interference can be divided into two types. Direct LiDAR interference means that the aggressor laser directly illuminates the ego LiDAR detector, whereas indirect LiDAR interference implies two LiDAR systems observing the same target. In both cases, we assume only perpendicular irradiance for simplicity. For direct LiDAR interference, this means exactly oppositely positioned LiDAR systems and for indirect LiDAR interference a target perpendicular to the ego LiDAR system. In the following, both LiDAR interference types are explained in detail.

For autonomous driving for example, direct LiDAR interference occurs if two vehicles stand or move in front of each other illuminating each other with laser signals. The image of the aggressor's apparent laser source area is transferred on the ego's pixels. Compared to the total field-of-view (FOV) of the ego LiDAR system, the apparent laser source area is tiny, typically in the order of micrometers [22]. Therefore, the aggressor laser signal probably hits only one pixel of the ego LiDAR detector. If the aggressor laser light hits exactly the pixel edge, alternatively two or four pixels are affected [23].

More critical is indirect LiDAR interference, where for example the ego and aggressor LiDAR system observe the same target. Multipath reflections with more than one target reflection can also lead to indirect LiDAR interference but this is not analyzed in this work. For identical LiDAR systems at the same target distance, the reflected laser signals look identical only differing with regards to their emission times. For indirect LiDAR interference, there are probably two indistinguishable laser signals showing up in the LiDAR measurement. In the following, we deliver more detailed considerations primarily concerning indirect LiDAR interference.

Direct LiDAR interference leads to higher intensities than indirect LiDAR interference. Since the received aggressor laser signal travels directly from the emitter to the receiver, the received irradiance is much higher than the irradiance by typical diffuse target reflections, which are ideally described by the Lambertian law. First, Lambertian reflections reduce the illumination by the target reflectance, e.g. $\rho = 80\%$. Second, Lambertian targets distribute the illumination omnidirectionally and not only back to the receiving LiDAR system. From the back-scattered Lambertian illumination, the LiDAR aperture cuts out

$$I_{\text{indirect}} = \rho \left(\frac{D}{2d}\right)^2 \approx 10^{-7}, \tag{2}$$

where $\rho = 80\%$ is the target reflectance, $D = 10\text{mm}$ is the aperture diameter and $d = 10\text{m}$ is the target distance [24]. Contrary to the reflection, the aggressor LiDAR system can illuminate a smaller FOV given by the horizontal and vertical emission angles θ_{H} and θ_{V} respectively, e.g. $\theta_{\text{H}} \times \theta_{\text{V}} = 60° \times 20°$. In this case, the fraction of illumination transmitting the aperture is given by

$$I_{\text{direct}} = \frac{\pi \left(\frac{D}{2}\right)^2}{4d^2 \tan\left(\frac{\theta_{\text{H}}}{2}\right) \tan\left(\frac{\theta_{\text{V}}}{2}\right)} \approx 10^{-6}, \tag{3}$$

where a homogenous rectangular illumination profile is assumed [25]. In this example, the ratio between indirect Lambertian reflection intensity I_{indirect} and direct illumination I_{direct} is given by

$$\frac{I_{\text{direct}}}{I_{\text{indirect}}} = \frac{\pi}{4\rho \tan\left(\frac{\theta_{\text{H}}}{2}\right) \tan\left(\frac{\theta_{\text{V}}}{2}\right)} \approx 10, \tag{4}$$

where the aperture diameter D and distance d cancelled out. Hence, direct LiDAR interference produces a higher maximum irradiance at the LiDAR detector than indirect LiDAR interference.

III. Appearance of LiDAR Interference in Measurements

In the following, we will discuss the expected signatures of LiDAR interference in TCSPC measurements in detail. Therefore, the appearance of the own ego laser signal and the aggressor laser signals in the measured histogram is analyzed. First, the probability density function (PDF) for LiDAR interference in the measured histogram is derived. Here, we limit our discussion to the first photon that is detected within one measurement cycle. The underlying photon processes of TCSPC measurements follow the Erlang distribution, which is derived from Poisson distribution and predicts the arrival time of the last photon for a specified total number of measured photons [26]–[28]. For the first photon, the Erlang distribution results in an exponential function $f(t) = r(t)\text{e}^{-\int r(t)\text{d}t}$ with time t and event rate $r(t)$ at the detector produced by incoming photons. For LiDAR, the event rate $r(t)$ is a time-dependent combination of background event rate r_{B} and laser event rate r_{L} as shown in Fig. 1. For simplicity, temporally rectangular laser pulse forms with pulse width t_{p} are assumed here. At the arrival time of the laser pulse t_{TOF}, the laser event rate r_{L} must be added to the background rate r_{B} during the laser pulse width t_{p}. Therefore, the PDF of a histogram with one laser

signal ($n_s = 1$) results into

$$P(t|n_s = 1) = \begin{cases} r_B e^{-r_B t}, & 0 \leqslant t < t_{TOF} \\ (r_B + r_L) e^{r_L t_{TOF}} e^{-(r_B + r_L)t}, & t_{TOF} \leqslant t < t_{TOF} + t_p \\ r_B e^{-r_L t_p} e^{-r_B t}, & t_{TOF} + t_p \leqslant t, \end{cases} \quad (6)$$

where t represents the time, which is discretized in the bin widths of the histogram during the LiDAR measurement [20]. These equations show that a constant background rate will appear as an exponentially decreasing signal in the measured LiDAR histogram as seen in Fig. 1. At the beginning of a measurement, the probability to measure the first photon is the highest and decreases with increasing waiting time, because it becomes more likely that the first photon has already been detected. With a larger TOF, it becomes more probable to measure background photons before the laser signal arrives, so that the measured intensity of later signals in the histogram is reduced, which is seen in Fig. 1 for the first signal in both histograms.

Each further laser signal is reduced by the probability already having detected the first photon during the previous laser signals, which is described for n_s laser signals in (5), as shown at the bottom of the page. For identical laser systems, the same laser pulse widths $t_{p,s} = t_p$ are given. If these laser systems observe the same target at the same distance, the reflected laser event rates $r_{L,s} = r_L$ can be assumed to be almost equal. Although ego and aggressor signal appear at different TOFs in the histogram, it is valid to use the same laser event rate r_L. The different TOFs are not representing different target distances leading to different laser event rates, as both systems can be assumed to have almost the same target distance in reality. The different TOFs in the histogram are only caused by the asynchronous measurement starts and thus different laser emission times. The PDF assumes discrete ascending laser signals with

$$t_{TOF,1} + t_p \leqslant t_{TOF,2}, \ldots, t_{TOF,n_s-1} + t_p \leqslant t_{TOF,n_s}, \quad (7)$$

where all aggressor TOFs represent no real target distances but apparent TOFs in the ego histogram. The PDF with these assumptions delivers the distribution of expected events showing the expected appearance of LiDAR interference in LiDAR measurement data. This knowledge is required to perform the following considerations and derive statements about the influence of LiDAR interference.

A. Influence of LiDAR Interference on Distance Determination

With the known appearance of LiDAR interference in the histogram, further data processing of the histogram can be discussed. For first-photon measurements, the first typical data processing step is the elimination of the exponential background [20]. Due to the pile-up effect at first-photon measurements, the remaining laser signals in the histogram have different heights even though they had equal intensities when arriving at the LiDAR system [29]. Although aggressor and ego signal are indistinguishable, we assume the worse case that the first high signal is the aggressor signal, whereas the second low signal is the ego signal. The first-photon measurement principle overemphasizes the earlier photons from the aggressor signal compared to later photons from the ego signal. Now, a simple constant fraction threshold as seen in Fig. 1 or maximum detection would always choose the aggressor signal in the histogram [30]. Additionally, the later ego signal below the detection threshold stays undetected so that unrecognized LiDAR interference occurs. If the first signal as aggressor signal is chosen, this standard LiDAR algorithm potentially leads to a false target distance determination.

Another interesting behavior is the independence of the aggressor signal position for the ego signal height. In Fig. 1, two different theoretically derived event distributions are shown. The orange histogram has an earlier and hence higher aggressor signal than the blue histogram. However, the ego laser signal height is identical for both histograms. The reason is that the first signal always has the same number of photons but following the pile-up effect of first-photon measurement principle, an earlier detection observes more of these laser photons. Instead, less background photons are measured so that the orange PDF falls below the blue PDF after the first laser signal. The total integral over the histogram up to the ego laser signal delivers the same number of detected photons for both distributions resulting into equal heights of the ego laser signals. The height of the ego laser signal is independent of the exact aggressor laser signal position. Therefore, the aggressor position must not be considered in further investigation and can be an arbitrary constant.

$$P(t|n_s) = \begin{cases} r_B e^{-r_B t}, & 0 \leqslant t < t_{TOF,1} \\ (r_B + r_L) e^{r_L t_{TOF,1}} e^{-(r_B + r_L)t}, & t_{TOF,1} \leqslant t < t_{TOF,1} + t_p \\ r_B e^{-r_L t_p} e^{-r_B t}, & t_{TOF,1} + t_p \leqslant t < t_{ext} \\ \vdots & \vdots \\ (r_B + r_L) e^{-(s-1) r_L t_p} e^{r_L t_{TOF,s}} e^{-(r_B + r_L)t}, & t_{TOF,s} \leqslant t < t_{TOF,s} + t_p \\ r_B e^{-(s-1) r_L t_p} e^{-r_B t}, & t_{TOF,s} + t_p \leqslant t < t_{TOF,s} \\ \vdots & \vdots \\ (r_B + r_L) e^{-(n_s-1) r_L t_p} e^{r_L t_{TOF,n_s}} e^{-(r_B + r_L)t}, & t_{TOF,n_s} \leqslant t < t_{TOF,n_s} + t_p \\ r_B e^{-(n_s-1) r_L t_p} e^{-r_B t}, & t_{TOF,n_s} + t_p \leqslant t < t_{TOF,n_s} \end{cases} \quad (5)$$

The probability of a detected photon occurring during a specified laser signal in the measured histogram is given by the number of photons during the laser signal width $n_{\text{signal},s}$ compared to the total number of detections in the histogram n_{hist}, which is equal or less than the number of measurements n_{meas}. Thus, the probability for a detected event to lie within laser signal s becomes

$$p_{\text{s}} = \frac{n_{\text{signal},s}}{n_{\text{hist}}} = \frac{n_{\text{meas}} \int_{t_{\text{TOF},s}}^{t_{\text{TOF},s}+t_{\text{p}}} P(t|n_{\text{s}})\,\text{d}t}{n_{\text{meas}} \int_{0}^{t_{\text{hist}}} P(t|n_{\text{s}})\,\text{d}t} = \frac{\text{e}^{-(s-1)r_{\text{L}}t_{\text{p}}}\left(1-\text{e}^{-(r_{\text{B}}+r_{\text{L}})t_{\text{p}}}\right)\text{e}^{-r_{\text{B}}t_{\text{TOF}}}}{1-\text{e}^{-n_{\text{s}}r_{\text{L}}t_{\text{p}}}\text{e}^{-r_{\text{B}}t_{\text{hist}}}}, \tag{8}$$

where t_{hist} is the total histogram length and each number of photons is calculated using the integrals over the PDF. For a correct distance determination based on the measured histogram, it is unimportant whether a detected photon at the correct TOF is a real laser photon reflected by the target or a randomly arriving background photon, which are indistinguishable. Therefore, the integration includes laser photons as well as background photons as long as they lie within the expected laser signal width.

For the example histograms in Fig. 1, this corresponds to an aggressor signal probability of 33% for the orange and 15% for the blue distribution as well as an ego signal probability of 2% in both cases. Statistically, this translates into a mean of 20 measured events within the second laser signal compared to $n_{\text{meas}} = 1000$ measurements in total, which fulfills the initially defined minimum SNR $k_{\text{SN,min}} = 3$ and hence is just barely detectable. The calculated signal probabilities confirm that more events lie within the first signal in the histogram. For each measurement, it must be proven whether the first signal in the histogram is the ego signal or not. Otherwise, LiDAR interference leads to a high risk of choosing an aggressor signal instead of the ego signal in the histogram resulting into a wrong distance determination. However, this work deals with the recognition of LiDAR interference occurrence, which is important to avoid assuming a single unknown signal as ego signal. The determination of the ego signal from multiple signals is part of related or future work.

B. Asynchronicity of LiDAR Systems

Another influence on the appearance of LiDAR interference can be the asynchronicity of LiDAR systems. The asychronicity of two LiDAR system's lasers can directly be caused by slightly different pulse repetition frequencies or different LiDAR system velocities, e.g. due to the vehicles on that the LiDAR systems are mounted.

LiDAR systems are affected by jitters meaning temporal fluctuations, e.g. of the laser emission time. The jitters of ego and aggressor signal in the measured ego histogram are both influenced by the jitter of the ego sensor. These identical jitter influences are uninteresting for the LiDAR interference analysis, because they do not lead to asynchronicity between the incoming signals. Potential differences between ego and aggressor signal are given by different jitters caused by different lasers. For our example LiDAR system, we measured these jitter differences. The jitter between the electrical trigger signal and the laser emission time was small compared to the electrical trigger uncertainty. Therefore, we only measured the trigger pulse repetition frequency differences over 1000 measurements each. For a set pulse repetition frequency of 10kHz corresponding to a period duration of 100 µs, the real pulse repetition frequency is measured for twelve different LiDAR system clocks directly via an oscilloscope. As expected, the standard deviation of the laser frequency is low with 62mHz and the measured mean frequency of 10.000 02kHz deviates only slightly from the ideal 10kHz. However, the corresponding mean period duration of 99.9998 µs with standard deviation 620ps is critical considering the bin width of this example LiDAR system, which is 312.5ps. Indeed, the minimum and maximum pulse repetition frequency even differ by 239mHz, which is equivalent to 2390ps.

The LiDAR system velocity has the same effect. Considering two LiDAR systems each on a vehicle with velocity 100km/h driving towards each other, the relative velocity is given by 200km/h. Within one laser cycle, this corresponds to a movement of 5.6mm or 37ps of the detected aggressor photons in the histogram. As this is small compared to a bin width of 312.5ps, this movement during one measurement is undetectable unless it happens exactly at the border of two bins. Accumulating 1000 of these aggressor photon measurements in the histogram, the drift of a single measurement becomes relevant with a total shift of 37ns corresponding to 5.6m. However, the pulse repetition frequency differences have a much higher impact on the LiDAR systems asynchronicity because they are generally higher than the vehicle velocity differences. Of course, both effects can combine so that both should be considered in general.

Assuming different LiDAR systems with different pulse repetition frequencies, their signals will be represented differently in one histogram. For low laser photon rates, the exponential shape of the laser signal in the histogram vanishes and the real laser pulse form is approximately seen in the histogram. Accumulating measurements, the ego signal will build up at the same position in average, whereas the aggressor signal systematically moves. For simplicity, we ignore the LiDAR sensor jitter here, which would affect the appearance of both signals additionally. If the measured aggressor signal TOF systematically drifts to lower or higher times, the accumulated aggressor signal becomes wider and lower as seen in Fig. 2. As mentioned before, the drift of a single measurement has little influence on the laser signal position in the histogram but a large number of accumulated measurements will show a large drift. For each measurement, a simple drift of two bin widths resulting in 625ps for the example LiDAR system is assumed, which approximately corresponds to the measured uncertainty of 620ps. The width of the accumulated ego signal is the pulse width of our example LiDAR system with 5ns, whereas the width of the accumulated aggressor signal becomes 62ns due to the drift, which is equivalent to a distance drift of 9m. In this ideal example event distribution with very low laser event rates, it is remarkable that the ego

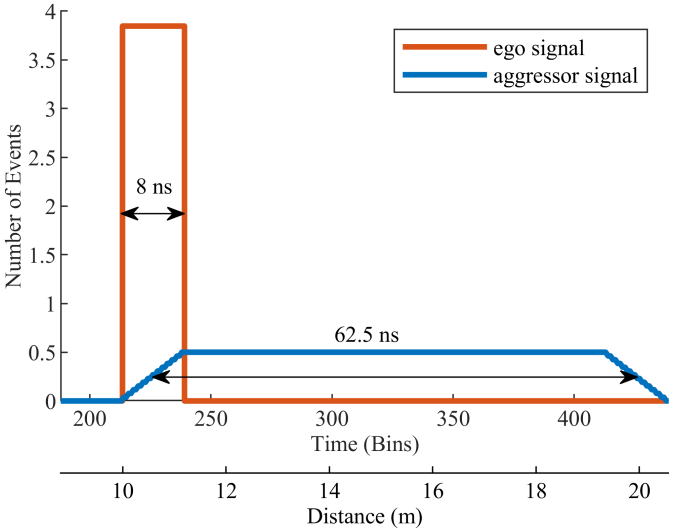

Fig. 2. Extended signal width of drifting aggressor signal due to asynchronicity of ego and aggressor LiDAR system with pulse repetition frequency difference of 625 ps.

signal has almost five events at its maximum, whereas the aggressor signal always has less than one event per bin. At the end, the pulse repetition frequency differences are crucial for LiDAR interference occurrence. Therefore, the measured pulse repetition frequencies of the used LiDAR systems are a good indicator. In the best case, all pulse repetition frequencies of the used LiDAR systems are completely different so that LiDAR interference is strongly suppressed.

IV. Unrecognized LiDAR Interference

Different conditions can lead to unrecognized LiDAR interference, which means that only the aggressor laser signal appears in the histogram, whereas the ego laser signal vanishes. This single measured signal can be wrongly assumed as signal emitted by the own LiDAR system because it cannot be classified into ego or aggressor signal without further analysis. Therefore, we refer to this effect as unrecognized LiDAR interference. The conditions for unrecognized LiDAR interference are investigated in the following. The PDF in (5) shows that the previous background and the previous laser signals reduce the following laser pulses. If the background event rate r_B and laser event rates r_L of previous signals are high enough, the last laser signals can vanish.

Corresponding to the minimum SNR already mentioned in the introduction, there exists a minimum TOF beyond which the ego signal will disappear. This TOF is called extinction TOF and is equivalent to a specific target distance that is called extinction distance in the following. Thus, LiDAR interference will always be detected if the real target distance is below the extinction distance. This knowledge avoids the output of a possibly wrong ego distance, whereas single signals in histograms will probably assumed as ego signal, although this might be wrong as well. However, for more than one signal, the target distance is still not known, as ego and aggressor signal are indistinguishable. The extinction distance d_ext is illustrated in Fig. 1, where it appears still detectable but in real measurements, each number of events per bin n will fluctuate with $\sqrt{n}$ due to Poisson statistics so that this noise makes the laser signal hard to detect [20], [24], [31]. Assuming a typical target for a specific LiDAR application, the probability of recognized LiDAR interference can be calculated with respect to the known extinction distance.

However, the extinction distance only describes the real target distance corresponding to the TOF of the second vanished ego laser signal. The first laser signal as aggressor has an arbitrary position in the measured histogram depending on the timing phase between the LiDAR systems. For the determination of the extinction distance, we calculate the SNR considering multiple laser signals in a histogram. After that, we investigate the unrecognized LiDAR interference with regards to the background as well as the laser event rate and the same for a specific LiDAR design meeting the eye safety conditions.

A. Signal-to-Noise Ratio

For the laser signal appearing at position s in the histogram, the SNR $k_{\mathrm{SN},s}$ is calculated from the number of laser photons $n_{\mathrm{L},s}$ and the measurement variance σ_s^2 with

$$k_{\mathrm{SN},s} = \frac{n_{\mathrm{L},s}}{\sigma_s} = \frac{n_{\mathrm{L},s}}{\sqrt{\sigma_{\mathrm{B},s}^2 + \sigma_{\mathrm{L},s}^2}} = \frac{n_{\mathrm{L},s}}{\sqrt{n_{\mathrm{B},s} + n_{\mathrm{L},s}}}. \tag{9}$$

In this equation, the total measurement variance σ_s^2 is replaced by the background variance $\sigma_{\mathrm{B},s}^2$ and the laser variance $\sigma_{\mathrm{L},s}^2$. Due to the underlying Poisson statistics, the variances $\sigma_{\mathrm{B},s}^2$ and $\sigma_{\mathrm{B},s}^2$ are the same as their corresponding number of photons $n_{\mathrm{B},s}$ and $n_{\mathrm{L},s}$ [20].

For the number of laser and background photons, the integral of the ideal PDF in (5) over the total laser pulse width is used. The SNR represents the ideal maximum laser information, which is achievable by filters or algorithms. There are filters only considering the bin with the maximum number of events but there are also algorithms considering the total pulse width, e.g. matched filters [30]. Besides, there are techniques considering the quantization problem as well [32]. In the future, the total signal might be extracted from the measurement by different techniques, filters and algorithms combined. Thus, the SNR is defined by the ideal laser signal representing the maximum laser information achievable by the different methods. The worse the detection method, the higher the required minimum SNR. With the number of measurements per histogram n_meas, the number of background photons n_B is determined to

$$\begin{aligned} n_{\mathrm{B},s} &= n_\mathrm{meas} \int_{t_{\mathrm{TOF},s}}^{t_{\mathrm{TOF},s}+t_\mathrm{p}} P(t|n_\mathrm{s})|_{r_\mathrm{L}=0}\,\mathrm{d}t \\ &= \mathrm{e}^{-(s-1)r_\mathrm{L}t_\mathrm{p}}\left(1-\mathrm{e}^{-r_\mathrm{B}t_\mathrm{p}}\right)\mathrm{e}^{-r_\mathrm{B}t_{\mathrm{TOF},s}}. \end{aligned} \tag{10}$$

Using this for the number of laser photons n_L results into

$$\begin{aligned} n_{\mathrm{L},s} &= n_\mathrm{meas} \int_{t_{\mathrm{TOF},s}}^{t_{\mathrm{TOF},s}+t_\mathrm{p}} P(t|n_\mathrm{s})\mathrm{d}t - n_\mathrm{B} \\ &= \mathrm{e}^{-(s-1)r_\mathrm{L}t_\mathrm{p}}\mathrm{e}^{-r_\mathrm{B}t_{\mathrm{TOF},s}}\left(\mathrm{e}^{-r_\mathrm{B}t_\mathrm{p}} - \mathrm{e}^{-(r_\mathrm{B}+r_\mathrm{L})t_\mathrm{p}}\right). \end{aligned} \tag{11}$$

Inserting both in (9), the SNR becomes

$$k_{\mathrm{SN},s} = \sqrt{n_{\mathrm{meas}} \mathrm{e}^{-(s-1)r_{\mathrm{L}}t_{\mathrm{p}}} \mathrm{e}^{-r_{\mathrm{B}}t_{\mathrm{TOF},s}}} \cdot \frac{\mathrm{e}^{-r_{\mathrm{B}}t_{\mathrm{p}}} - \mathrm{e}^{-(r_{\mathrm{B}}+r_{\mathrm{L}})t_{\mathrm{p}}}}{\sqrt{1-\mathrm{e}^{-(r_{\mathrm{B}}+r_{\mathrm{L}})t_{\mathrm{p}}}}}. \quad (12)$$

For low background event rates as well as low laser event rates, the approximations $r_{\mathrm{B}} \ll {}^{1}/_{t_{\mathrm{p}}}$ and $(r_{\mathrm{B}}+r_{\mathrm{L}}) \ll {}^{1}/_{t_{\mathrm{p}}}$ allow to use the simpler form

$$k'_{\mathrm{SN},s} = \sqrt{n_{\mathrm{meas}} t_{\mathrm{p}} \mathrm{e}^{-(s-1)r_{\mathrm{L}}t_{\mathrm{p}}} \mathrm{e}^{-r_{\mathrm{B}}t_{\mathrm{TOF},s}}} \frac{r_{\mathrm{L}}}{\sqrt{r_{\mathrm{B}}+r_{\mathrm{L}}}}, \quad (13)$$

where the similarity to (9) is seen. For these low rates, the possibility to detect a photon during laser pulse width t_{p} is very low and there might be measurements without any triggered event at all at the sensor. For pulse width $t_{\mathrm{p}} = 8\mathrm{ns}$ and rates $r_{\mathrm{L}} = r_{\mathrm{B}} = 5 \cdot 10^{6}$ Hz, the SNR deviation of the approximated SNR is given by

$$\Delta k_{\mathrm{SN},s} = \frac{k'_{\mathrm{SN},s} - k_{\mathrm{SN},s}}{k_{\mathrm{SN},s}} = 4\%, \quad (14)$$

and for rates $r_{\mathrm{L}} = r_{\mathrm{B}} = 10^{7}$ Hz it might be still acceptable with $\Delta k_{\mathrm{SN},s} = 8\%$. In the following, we use the unapproximated form. The unrecognized LiDAR interference is evaluated for only two LiDAR systems meaning a total number of LiDAR signals $n_{\mathrm{s}} = 2$. As worst case, the ego signal is assumed to be the last, which is $s = 2$ in this case. For more than two LiDAR systems, the probability of unrecognized LiDAR interference will be even higher und the extinction distance shorter. From now on, the SNR of the ego signal is meant with $k_{\mathrm{SN}} = k_{\mathrm{SN},s=2}$. Inserting this into (12), the equation can be solved for the extinction distance or extinction TOF of the ego signal, which is the vanishing second laser signal $t_{\mathrm{TOF},2} = t_{\mathrm{ext}}$, resulting into

$$t_{\mathrm{ext}} = \frac{1}{r_{\mathrm{B}}} \cdot \ln\left(\frac{n_{\mathrm{meas}}}{k_{\mathrm{SN}}^2} \mathrm{e}^{-r_{\mathrm{L}}t_{\mathrm{p}}} \frac{\left(\mathrm{e}^{-r_{\mathrm{B}}t_{\mathrm{p}}} - \mathrm{e}^{-(r_{\mathrm{B}}+r_{\mathrm{L}})t_{\mathrm{p}}}\right)^2}{1-\mathrm{e}^{-(r_{\mathrm{B}}+r_{\mathrm{L}})t_{\mathrm{p}}}} \right). \quad (15)$$

This is transformed to the extinction distance d_{ext} by the well-known equation (1). The extinction distance is shown in Fig. 3 for different values of SNR k_{SN}. As expected, the extinction distance increases for a decreasing SNR meaning a better distance determination method. As the SNR depends on the number of measurements per histogram n_{meas}, the extinction distance increases also with the number of measurements. The minimum number of measurements $n_{\mathrm{meas,min}}$ to detect the ego signal at all is given for an ego signal position right after the aggressor signal. For an aggressor pulse width t_{p}, the earliest ego TOF is thus equal to the aggressor laser pulse width $t_{\mathrm{TOF},2} = t_{\mathrm{p}}$. Considering a minimum SNR $k_{\mathrm{SN,min}}$, this results into the inverse SNR equation

$$n_{\mathrm{meas,min}} = k_{\mathrm{SN,min}}^2 \frac{\mathrm{e}^{(r_{\mathrm{B}}+r_{\mathrm{L}})t_{\mathrm{p}}} - 1}{\left(\mathrm{e}^{-r_{\mathrm{B}}r_{\mathrm{p}}} - \mathrm{e}^{-(r_{\mathrm{B}}+r_{\mathrm{L}})t_{\mathrm{p}}}\right)^2}, \quad (16)$$

which is marked by filled circles in Fig. 3. Summarized, the higher the number of measurements and the lower the still detectable SNR, the better the LiDAR distance measurement and hence the lower the LiDAR interference probability.

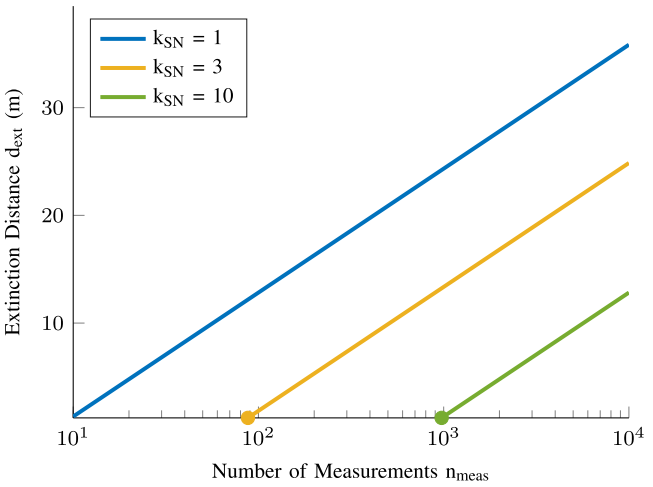

Fig. 3. Extinction distance d_{ext} depending of the number of measurements per histogram n_{meas} for different SNRs: lowest SNR $k_{\mathrm{SN}} = 1$, average SNR $k_{\mathrm{SN}} = 3$ and SNR $k_{\mathrm{SN}} = 10$ for easily evaluable signals. The minimum number of measurements $n_{\mathrm{meas,min}}$ for a barely recognizable ego signal behind the aggressor signal is marked as filled circle each.

B. Background and Laser Event Rate

Background and laser event rate strongly influence the unrecognized LiDAR interference as seen in Fig. 4. There is a maximum background event rate $r_{\mathrm{B,max}}$ for a given laser event rate r_{L} allowing recognizable LiDAR interference, which can be calculated by

$$r_{\mathrm{B,max}} = r_{\mathrm{L}} \frac{\frac{n_{\mathrm{meas}}}{k_{\mathrm{SN}}^2} r_{\mathrm{L}} t_{\mathrm{p}} - 1}{1 + 2\frac{n_{\mathrm{meas}}}{k_{\mathrm{SN}}^2} r_{\mathrm{L}}^2 t_{\mathrm{p}}^2}. \quad (17)$$

In Fig. 4, the maximum background rate is $r_{\mathrm{B}} = 100\mathrm{MHz}$. The background rate of $r_{\mathrm{B}} = 1\mathrm{GHz}$ already lies out of bounds because it produces negative extinction distances meaning no recognizable ego signal at all.

The laser event rate of ego and aggressor signal is another relevant parameter for LiDAR interference. On the one hand, a higher ego laser event rate leads to a potentially higher ego signal. On the other hand, a too high aggressor laser event rate will more often be detected as first photon so that the ego signal is reduced. If the aggressor signal is so high that it produces a photon detection with a probability approaching 100%, even arbitrarily high ego laser event rates would still not be detectable. This trade-off delivers an ideal laser event rate with maximum extinction distance d_{ext} and hence the lowest probability of unrecognized LiDAR interference, which corresponds to the maxima in Fig. 4. The ideal maximum laser event rate $r_{\mathrm{L,ideal}}$ is received numerically by solving

$$2\mathrm{e}^{-(2r_{\mathrm{B}}+r_{\mathrm{L,ideal}})t_{\mathrm{p}}} + \mathrm{e}^{(r_{\mathrm{L,ideal}}-r_{\mathrm{B}})t_{\mathrm{p}}} = 3\mathrm{e}^{-r_{\mathrm{B}}t_{\mathrm{p}}}. \quad (18)$$

Similar to (13), this equation is approximated in second order for low background and laser event rates to

$$r_{\mathrm{L,ideal}} \approx \frac{1}{3t_{\mathrm{p}}} - r_{\mathrm{B}} + \sqrt{\left(\frac{1}{3t_{\mathrm{p}}} + r_{\mathrm{B}}\right)^2 - 2r_{\mathrm{B}}^2} \approx \frac{2}{3t_{\mathrm{p}}}, \quad (19)$$

where the stronger approximation $r_{\mathrm{B}} \ll {}^{1}/_{3t_{\mathrm{p}}}$ was applied in a second step. This approximation is independent of background

event rate r_B, i.e. only the aggressor laser width t_p is relevant. For background event rate $r_B = 10^7$ Hz, the deviations are $\Delta r_{L,ideal} = 1 \times 10^7 \text{Hz} \mathrel{\widehat{=}} 10\%$ for both approximations, which is seen by the slightly decreased marker in Fig. 4. For background with 10^6 Hz, both deviations just fall below 5%, so that the approximations can be safely used until $r_B = 10^6$ Hz. For the highest possible background $r_B = 10^8$ Hz, only the exact numerical solution without approximations is valid, but the ideal maximum laser event rate is still near $r_{L,ideal} = 10^8$ Hz. For even higher background $r_{L,ideal} = 10^9$ Hz, LiDAR interference becomes unrecognizable, as it is higher than the maximum possible laser event rate of 6×10^8Hz leading to a very low SNR. Equivalent to the required minimum number of measurements in the section before, the minimum laser event rate $r_{L,min}$ is determined by

$$r_{L,min} \approx \frac{k_{SN}^2}{2n_{meas}t_p} e^{r_B t_{ext}} + \frac{1}{t_p}\sqrt{\left(r_B t_p + \frac{k_{SN}^2}{2n_{meas}} e^{r_B t_{ext}}\right)^2 - r_B^2 t_p^2}, \quad (20)$$

including the approximations of low background and laser event rates. If all other LiDAR system parameters determining the laser event rate r_L are fixed, these equations deliver a minimum and an optimal laser event rate r_L or corresponding laser pulse width t_p. Assuming a typical laser event rate of $r_L = 100$MHz, the ideal laser pulse width is given by (19) to $t_p = 6.7$ns. The equation can be applied as well in the other direction. For a LiDAR system with pulse width $t_p = 3$ns, the ideal laser event rate is $r_L = 200$MHz. Choosing all other LiDAR system parameters in the LiDAR range equation leads to a perfect target with defined reflectance ρ and distance d, which has the lowest LiDAR interference. For example, the working environment of a robot can be designed with these perfect targets. Besides the ideal LiDAR interference circumstances, the compliance with the eye safety limit must be ensured additionally for a LiDAR system design, which could restrict the allowed laser pulse width as described in the next section.

C. LiDAR Interference for a Specific LiDAR System

Previously, we used only laser event rates, which describe no specific LiDAR system or target but show general effects. The equations can be used to develop a specific LiDAR system with defined parameters or to optimally reduced LiDAR interference. However, a LiDAR system cannot be optimized only with regards to the performance or lowest LiDAR interference. The eye safety of the used laser must always be considered. The derived equations are completed by the boundary condition of eye safety now and compared to the calculations without eye safety. For a given laser event rate $r_L = $ const., the influence of the laser pulse width t_p is shown in Fig. 5. In this case, the relation to the general case of n_s laser signals is easy and hence explicitly given here. The resulting laser pulse width is numerically received by solving

$$\frac{2r_L}{e^{r_L t_p} - 1} + \frac{r_B + r_L}{1 - e^{(r_B + r_L)t_p}} = 2 \cdot r_B + n_s r_L. \quad (21)$$

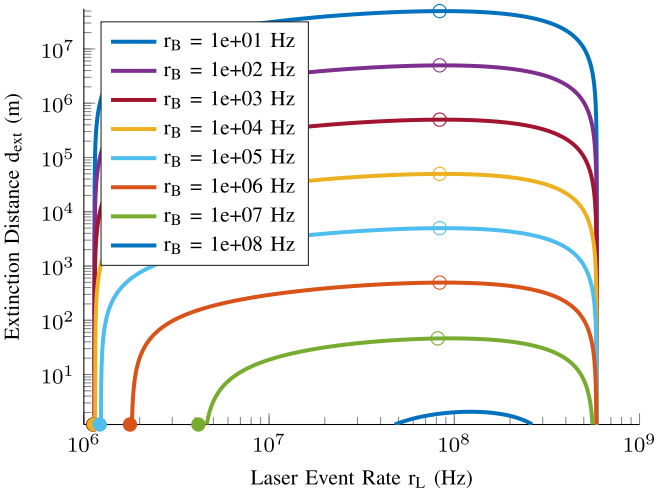

Fig. 4. Extinction distance d_{ext} depending on laser event rate r_L and background event rate r_B. Approximated minimum laser event rates are marked by filled circles and approximated ideal laser event rates are marked as empty circles.

The optical laser power of the LiDAR systems is restricted by the eye safety in the mandatory norm IEC 60825 [33]. This eye safety claims a maximum laser energy, which can be simplified to $r_L t_p = $ const. for a fixed number of measurements. In all figures before, the laser event rate is constant, to be read off for the combination of a given LiDAR system and specified target properties. Alternatively, the reflected photon rates can be adjusted to the target distance so that only the LiDAR system properties are fixed. Now, the considered laser event rate directly depends on the extinction distance d_{ext} given by

$$r_L(d_{ext}) = \frac{x_d}{d_{ext}^2} = \frac{x_t}{t_{ext}^2}, \quad (22)$$

where the proportion factor x_d is defined with respect to the extinction distance d_{ext} or x_t with respect to the corresponding extinction TOF t_{ext}. These factors are determined by the LiDAR range equation in [24] resulting into

$$x_t = \frac{4x_d}{c^2} = \frac{4}{c^2}\frac{\Phi_L}{\Omega_L}\rho T \frac{1}{4k^2} A_{px}\eta_{PDE}\frac{\lambda}{hc}, \quad (23)$$

where c is the speed of light, Φ_L is the optical laser power, Ω_L is the laser solid angle based on the laser opening angles, ρ is the target reflectance, T is the transmission factor by optics or atmosphere, k is the receiving optics f-number, A_{px} is the pixel area, η_{PDE} is the photon detection efficiency (PDE), λ is the wavelength and h is the Planck constant. Considering this dependency, the extinction TOF can only be given numerically by solving

$$\frac{n_{meas}}{k_{SN}^2} = e^{\frac{x}{t_{ext}^2}t_p} e^{r_B t_{ext}^2} \frac{1 - e^{-(r_B + \frac{x}{t_{ext}^2})t_p}}{\left(e^{-r_B t_p} - e^{-(r_B + \frac{x}{t_{ext}^2})t_p}\right)^2}. \quad (24)$$

As seen in Fig. 5, the extinction distance decreases if the laser event rate includes eye safety and increasing target distances. For the chosen LiDAR system parameters of the red line, the optimal laser pulse width to avoid LiDAR interference is in the order of ns, which corresponds to the current state of the art. Laser pulse widths below lead to no further remarkable

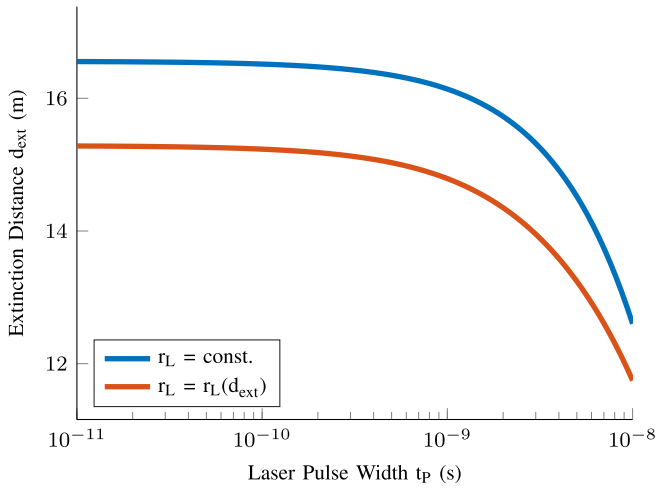

Fig. 5. Extinction distance d_{ext} depending on the laser pulse width t_p for a constant laser event rate r_L = const. or related to eye safety by $r_L = r_L(d_{ext})$.

improvement of the extinction distance. If a LiDAR system will be designed and the parameters are still unknown, the derived equations can be used without considering eye safety and the connection between intensity and target distance. This is helpful to find the ideal working point for a belonging laser event rate r_L. From that, the LiDAR system parameters can be chosen. If the LiDAR system parameters are already chosen, the equations considering eye safety and target distance can be applied to analyze the LiDAR interference of the designed LiDAR system. Therefore, depending on the desired approach, a constant laser event rate r_L = const. or a laser event rate depending on the target distance d with $r_L(d_{ext})$ is appropriate here, which can be applied on all other derived equations as well.

V. Solutions

In the following, we present possible solutions to avoid incorrect measurements due to LiDAR interference for TCSPC flash LiDAR systems, which can be combined as well.

A. Recognition of LiDAR Interference

The first challenge is to recognize LiDAR interference. As shown before, the probability of unrecognized LiDAR interference is already influenced by the LiDAR system design. Therefore, the background event rate or laser event rate received by the LiDAR system can be optimized for the derived ideal operating point in section IV-B, for example under the assumption of average target properties of the respective application. Keeping the laser event rate constant, the background event rate is difficult to control except by bandpass filters or coincidence detection [34]. It is easier to optimize the laser event rate by the optical laser power Φ_L or the opening angles of the laser field-of-illumination (FOI) $\theta_H \times \theta_V$ given by

$$r_L \propto \frac{\Phi_L}{4 \tan\left(\frac{\theta_H}{2}\right) \tan\left(\frac{\theta_V}{2}\right)}, \tag{25}$$

which is part of the LiDAR equation [20], [24], [25]. Furthermore, both event rates can be increased by the following parameters of the same equation: f-number, transmissions of optics, pixel area, PDE or laser wavelength. Increasing both rates, the additional background can be eliminated again using appropriate techniques, filters or algorithms, whereas the laser event rate could stay as desired. As described in section IV-C, the respecting eye-safety conditions must always be fulfilled while optimizing the LiDAR system for the lowest probability of unrecognized LiDAR interference.

Unrecognized LiDAR interference can still exist for optimized LiDAR systems, but there are some hints to recognize it afterwards, which can be used to express a warning to the user or initialize methods to prove the presence of LiDAR interference. In section IV-B, we have shown the maximum background event rate for recognized LiDAR interference. Hence, everything beyond probably leads to unrecognized LiDAR interference. Furthermore, the extinction distance itself depending on background and laser event rate can be used as a hint. Assuming an unaffected measurement resulting in a target distance larger than the extinction distance, a sudden change to a lower distance is also a hint for unrecognized LiDAR interference. The true target distance is still beyond the extinction distance and hence no longer seen in the histogram in the presence of the aggressor signal. To search for this invisible target signal, the measurement window can be opened after the known signal by time gating [35] so that a potential signal should become visible. Apart from that, the case of targets beyond the extinction distance can be excluded by other sensors like radio detection and ranging (radar). When unrecognized LiDAR interference can be excluded, the occurrence of LiDAR interference is expected to be clearly seen in the histogram.

An indication only for direct LiDAR interference is to check if the intensities measured at the LiDAR system are much higher than possible by a regular target reflection. In section II, we calculated the intensity difference between direct LiDAR interference and the indirect one based on a diffuse Lambertian target reflection. If the intensity at the LiDAR system is higher than that of the brightest target with $\rho = 100\%$ reflectance, there is probably LiDAR interference occurring. Transferred to the expected event distribution of the measured histogram [20], the maximum limit for a laser signal consists of a simple exponential line in the histogram at

$$f(t) = t_{bin} n_{meas} (r_B + r_L) e^{-r_B t_{TOF}}, \tag{26}$$

where r_L is the laser event rate for a Lambertian target with 100% reflectance calculated by the common LiDAR equation [24]. If the signal exceeds this limit, a warning for direct LiDAR interference should be given. For non-diffuse targets like retroreflectors of traffic signs, a second even higher exponential warning limit is suitable representing a strong sign for direct LiDAR interference if it is exceeded. This mechanism allows for a fast evaluation of the current LiDAR interference probability but requires further information to validate indications of LiDAR interference.

B. Reduction of LiDAR Interference

For the reduction of LiDAR interference, the asynchronicity analyzed in section III-B is useful. Therefore, a conceivable

solution would be intentional pulse repetition frequency differences for a series production of laser systems. As mentioned before, it would be sufficient to maximally differ in order of the bin width. For a bin width of $t_{\mathrm{bin}} = 312.5$ps, the laser frequencies $f_1 = 10$kHz and $f_2 = 9.999\,97$kHz are already sufficiently different to avoid LiDAR interference. For millions of LiDAR systems, different frequencies for every LiDAR system might be difficult. To get different laser frequencies easily for all LiDAR systems, the laser difference can be imitated by an intentional random time delay of the own pulse repetition frequency, which is also called PPM [12]–[17]. Due to eye safety, the laser can only be delayed so that the pulse repetition frequency is never increased. However, a time delay of a bin width is negligible compared to typical pulse repetition frequencies. If a reduction of the aggressor signal is achieved, the ego signal will be the highest signal in the histogram and easy to choose. However, if the LiDAR system still measures more than one possible signal in the histogram, the own laser position is found by a repeated measurement with disabled ego laser. Then, the disappeared signal was the ego signal. For cooperative pulsed LiDAR systems, additional methods like space-division multiple access (SDMA), wavelength-division multiple access (WDMA) or time-division multiple access (TDMA) can be applied [36] but for uncontrolled environments with many pulsed LiDAR systems, only CDMA or PPM is sufficient [37]. For TCSPC, the pile-up effect avoids the measurement of exact pulse forms so that classical CDMA is difficult to apply and even only PPM seems to remain as a suitable solution.

VI. Conclusion

Mutual LiDAR interference of LiDAR systems is an important safety issue, especially in autonomous driving applications. In this work, we introduced two LiDAR interference types, of which indirect LiDAR interference is more difficult to detect and hence more dangerous than direct LiDAR interference. For the further investigations, we assumed identical TCSPC flash LiDAR systems using dTOF with short laser pulses and first-photon measurement principle.

In some cases, occurring LiDAR interference leads to dangerous situations. For detailed investigations, the PDF for measured histograms showing LiDAR interference has been derived. Consecutive laser signals with equal emission intensities represent the most critical situation, because in the measured histogram, the first signal is always the highest whether it is ego or aggressor signal. Otherwise, the aggressor signal can appear strongly reduced compared to the ego signal due to slightly different ego and aggressor pulse repetition frequency.

A huge risk is unrecognized LiDAR interference, where background and aggressor signal reduce the ego signal until invisibility so that only the aggressor signal is seen. The extinction distance for real targets is derived, from which the target stays invisible so that LiDAR interference becomes unrecognized. This increases with the number of accumulated measurements but also with the required minimum SNR for the used filters and algorithms to determine the target distance by the measured histogram. Additionally, we derived the ideal laser event rate for the lowest probability of unrecognized LiDAR interference, which is high enough to increase the ego signal above the background distribution but low enough that the previous aggressor signal does not extinct the later ego signal. We found an approximation that shows a direct connection between this ideal laser event rate and the optimal laser pulse width, which enables an ideal LiDAR system design with regards to LiDAR interference.

For the analysis of specific LiDAR parameters and target, the laser event rate must be chosen with regards to intensity loss due to higher target distances and allowed eye safety limit. As expected, high laser event rates are advantageous and restrictions like eye safety as well as large target distances decrease the extinction distance of unrecognized LiDAR interference. The derived equations deliver the LiDAR system properties with regards to LiDAR interference. Finally, possible solutions are provided for the recognition and reduction of LiDAR interference.

Symbols

Symbol	Value	Unit	Description
d_{ext}	0..300	m	extinction distance
d	0..300	m	target distance
$k_{\mathrm{SN,min}}$	3	–	min. SNR for detection
n_{meas}	1000	–	no. of measurements per hist.
n_{s}	2	–	no. of laser signals in hist.
r_{B}	30	MHz	background event rate
r_{L}	100	MHz	laser event rate
t_{TOF}	0..2	µs	time-of-flight (TOF)
t_{ext}	0..2	µs	extinction time
t_{p}	8	ns	laser pulse width
t	0..2	µs	time

References

[1] J. Eom, G. Kim, and Y. Park, "Mutual interference potential and impact of scanning LiDAR according to the relevant vehicle applications," *Proc. SPIE*, vol. 11005, May 2019, Art. no. 110050I.

[2] G. B. Popko, T. K. Gaylord, and C. R. Valenta, "Geometric approximation model of inter-LiDAR interference," *Opt. Eng.*, vol. 59, no. 3, p. 1, Mar. 2020.

[3] M. Perenzoni, D. Perenzoni, and D. Stoppa, "A 64×64-pixels digital silicon photomultiplier direct TOF sensor with 100-MPhotons/s/pixel background rejection and imaging/altimeter mode with 0.14% precision up to 6 km for spacecraft navigation and landing," *IEEE J. Solid-State Circuits*, vol. 52, no. 1, pp. 151–160, Jan. 2017.

[4] S.-Y. Tsai, Y.-C. Chang, and T.-H. Sang, "SPAD LiDARs: Modeling and algorithms," in *Proc. 14th IEEE Int. Conf. Solid-State Integr. Circuit Technol. (ICSICT)*, Oct. 2018, pp. 1–4.

[5] A. Tontini, L. Gasparini, and M. Perenzoni, "Numerical model of SPAD-based direct time-of-flight flash LIDAR CMOS image sensors," *Sensors*, vol. 20, no. 18, p. 5203, Sep. 2020.

[6] P. B. Coates, "The correction for photon 'pile-up' in the measurement of radiative lifetimes," *J. Phys. E, Sci. Instrum.*, vol. 1, no. 8, pp. 878–879, Aug. 1968.

[7] A. Gupta, A. Ingle, A. Velten, and M. Gupta, "Photon-flooded single-photon 3D cameras," in *Proc. IEEE/CVF Conf. Comput. Vis. Pattern Recognit. (CVPR)*, Jun. 2019, pp. 6763–6772.

[8] K. Pasquinelli, R. Lussana, S. Tisa, F. Villa, and F. Zappa, "Single-photon detectors modeling and selection criteria for high-background LiDAR," *IEEE Sensors J.*, vol. 20, no. 13, pp. 7021–7032, Jul. 2020.

[9] I. Hwang and C. Lee, "Mutual interferences of a true-random LiDAR with other LiDAR signals," *IEEE Access*, vol. 8, pp. 124123–124133, 2020.

[10] B. Büttgen, M.-A. E. Mechat, F. Lustenberger, and P. Seitz, "Pseudonoise optical modulation for real-time 3-D imaging with minimum interference," *IEEE Trans. Circuits Syst. I, Reg. Papers*, vol. 54, no. 10, pp. 2109–2119, Oct. 2007.
[11] T. Fersch, R. Weigel, and A. Koelpin, "A CDMA modulation technique for automotive time-of-flight LiDAR systems," *IEEE Sensors J.*, vol. 17, no. 11, pp. 3507–3516, Mar. 2017.
[12] D. U. Fluckiger, B. F. Boland, and E. Marcus, "Optimal pseudorandom pulse position modulation ladar waveforms," *Appl. Opt.*, vol. 54, no. 9, pp. 2183–2186, Mar. 2015.
[13] L. Carrara and A. Fiergolski, "An optical interference suppression scheme for TCSPC flash LiDAR imagers," *Appl. Sci.*, vol. 9, no. 11, p. 2206, May 2019.
[14] A. R. Ximenes, P. Padmanabhan, M.-J. Lee, Y. Yamashita, D.-N. Yaung, and E. Charbon, "A modular, direct time-of-flight depth sensor in 45/65-nm 3-D-stacked CMOS technology," *IEEE J. Solid-State Circuits*, vol. 54, no. 11, pp. 3203–3214, Nov. 2019.
[15] P. Du, F. Zhang, Z. Li, Q. Liu, M. Gong, and X. Fu, "Single-photon detection approach for autonomous vehicles sensing," *IEEE Trans. Veh. Technol.*, vol. 69, no. 6, pp. 6067–6078, Jun. 2020.
[16] T.-H. Sang, N.-K. Yang, Y.-C. Liu, and C.-M. Tsai, "A method for fast acquisition of photon counts for SPAD LiDAR," *IEEE Sensors Lett.*, vol. 5, no. 3, pp. 1–4, Mar. 2021.
[17] Y. Yu *et al.*, "Detection probability analysis of true random coding photon counting LiDAR," *Photonics*, vol. 8, no. 12, p. 545, Nov. 2021.
[18] H. Seo *et al.*, "Direct TOF scanning LiDAR sensor with two-step multievent histogramming TDC and embedded interference filter," *IEEE J. Solid-State Circuits*, vol. 56, no. 4, pp. 1022–1035, Apr. 2021.
[19] G. Kim and Y. Park, "Suitable combination of direct intensity modulation and spreading sequence for LIDAR with pulse coding," *Sensors*, vol. 18, no. 12, p. 4201, Nov. 2018.
[20] M. Beer, "SPAD-basierte Sensoren für die laufzeitbasierte distanzmessung bei hoher hintergrundlichtintensität," Ph.D. dissertation, Dept. Electron. Compon. Circuits, Fac. Elect. Eng. Inf. Technol., Univ. Duisburg-Essen, Duisburg, Germany, 2018. [Online]. Available: https://duepublico2.uni-due.de/servlets/MCRFileNodeServlet/duepublico_derivate_00046797/Diss_Beer.pdf
[21] A. Buchner *et al.*, "Analytical evaluation of signal-to-noise ratios for avalanche- and single-photon avalanche diodes," *Sensors*, vol. 21, no. 8, p. 2887, Apr. 2021.
[22] S. Yao and K. Ji, "Synthetic aperture laser imaging system: A review," *Proc. SPIE*, vol. 2888, pp. 392–398, Sep. 1996.
[23] A. Eisele, "Millimeter-precision laser rangefinder using a low-cost photon counter," Ph.D. dissertation, Karlsruhe Inst. Technol., Karlsruhe, Germany, 2013.
[24] P. Seitz and A. J. Theuwissen, *Single-Photon Imaging*. Berlin, Germany: Springer, 2011.
[25] P. Padmanabhan, C. Zhang, and E. Charbon, "Modeling and analysis of a direct time-of-flight sensor architecture for LiDAR applications," *Sensors*, vol. 19, no. 24, p. 5464, Dec. 2019.
[26] S. M. Ross, *Stochastic Processes* (Wiley Series in Probability and Statistics). Hoboken, NJ, USA: Wiley, 1996.
[27] P. Gatt, S. Johnson, and T. Nichols, "Geiger-mode avalanche photodiode ladar receiver performance characteristics and detection statistics," *Appl. Opt.*, vol. 48, no. 17, pp. 3261–3276, Jun. 2009.
[28] E. G. Kolomiitsev, A. A. Kovalev, V. M. Nikitin, and V. N. Fomin, "Detection of weak optical signals in LiDAR measurements under noise conditions," *Atmos. Ocean. Opt.*, vol. 24, no. 3, pp. 223–230, Jun. 2011.
[29] A. K. Pediredla, A. C. Sankaranarayanan, M. Buttafava, A. Tosi, and A. Veeraraghavan, "Signal processing based pile-up compensation for gated single-photon avalanche diodes," 2018, *arXiv:1806.07437*.
[30] C. A. Grönwall, O. K. Steinvall, F. Gustafsson, and T. R. Chevalier, "Influence of laser radar sensor parameters on range-measurement and shape-fitting uncertainties," *Opt. Eng.*, vol. 46, no. 10, pp. 1–11, Oct. 2007.
[31] S. Pellegrini, G. S. Buller, J. M. Smith, A. M. Wallace, and S. Cova, "Laser-based distance measurement using picosecond resolution time-correlated single-photon counting," *Meas. Sci. Technol.*, vol. 11, no. 6, pp. 712–716, Jun. 2000.
[32] J. Rapp, R. M. A. Dawson, and V. K. Goyal, "Improving LiDAR depth resolution with dither," in *Proc. 25th IEEE Int. Conf. Image Process. (ICIP)*, 2018, pp. 1553–1557.
[33] *Safety of Laser Products*, IEC Standard 60825-1, 2014.
[34] J. Haase, M. Beer, O. Schrey, J. Ruskowski, W. Brockherde, and H. Vogt, "Measurement concept for direct time-of-flight sensors at high ambient light," *Proc. SPIE*, vol. 10926, pp. 102–108, Feb. 2019.
[35] J. F. Haase, A. Buchner, S. Grollius, J. Ruskowski, and H. Vogt, "Measurement concept to reduce environmental impact in direct time-of-flight LiDAR sensors," *Proc. SPIE*, vol. 11288, pp. 60–68, Jan. 2020.
[36] B. Buttgen and P. Seitz, "Robust optical time-of-flight range imaging based on smart pixel structures," *IEEE Trans. Circuits Syst. I, Reg. Papers*, vol. 55, no. 6, pp. 1512–1525, Jun. 2008.
[37] F. Villa, F. Severini, F. Madonini, and F. Zappa, "SPADs and SiPMs arrays for long-range high-speed light detection and ranging (LiDAR)," *Sensors*, vol. 21, no. 11, p. 3839, Jun. 2021.

Sara Grollius received the bachelor's and Master of Science degrees in physics from the University of Wuppertal, Germany. She is currently pursuing the Ph.D. degree in electrical engineering with the Fraunhofer Institute for Microelectronic Circuits and Systems (IMS), Duisburg. Her topic is about the quality and reliability of light detection and ranging (LiDAR) systems, which determine target distances by the principle of direct time-of-flight.

Andre Buchner received the bachelor's and master's degrees in electrical engineering from the University of Duisburg-Essen in 2016 and 2019, respectively, specializing in micro- and optoelectronics. He is pursuing the Ph.D. degree with the Fraunhofer Institute for Microelectronic Circuits and Systems (IMS) on the topic of algorithms for single-photon avalanche diode-based light detection and ranging (LiDAR) systems. His interests incorporate programming, optics, and embedded systems.

Manuel Ligges received the Diploma and Ph.D. degrees in physics from the University of Duisburg-Essen. Until 2019, he has worked as a Research Assistant and an Assistant Professor of Solid-State Physics. He leads the Group of Optical Systems, Fraunhofer Institute for Microelectronic Circuits and Systems (IMS), Duisburg.

Anton Grabmaier studied physics at the University of Stuttgart and specialized in semiconductor physics and measurement technology. His dissertation was focused on laser diodes. Since 2006, he has been a Professor at the University of Duisburg-Essen. He is working as the Director of the Fraunhofer Institute for Microelectronic Circuits and Systems (IMS), Duisburg.